AIAA-2008-4403

38th AIAA Fluid Dynamics Conference and Exhibit, June 23 – 26, 2008, Seattle, WA

Turbulence Model Behavior in Low Reynolds Number Regions of Aerodynamic Flowfields

Christopher L. Rumsey*

NASA Langley Research Center, Hampton, VA 23681-2199

Philippe R. Spalart†

Boeing Commercial Airplanes, Seattle, WA 98124

The behaviors of the widely-used Spalart-Allmaras (SA) and Menter shear-stress transport (SST) turbulence models at low Reynolds numbers and under conditions conducive to relaminarization are documented. The flows used in the investigation include 2-D zero pressure gradient flow over a flat plate from subsonic to hypersonic Mach numbers, 2-D airfoil flow from subsonic to supersonic Mach numbers, 2-D subsonic sink-flow, and 3-D subsonic flow over an infinite swept wing (particularly its leading-edge region). Both models exhibit a range over which they behave "transitionally" in the sense that the flow is neither laminar nor fully turbulent, but these behaviors are different: the SST model typically has a well-defined transition location, whereas the SA model does not. Both models are predisposed to delayed activation of turbulence with increasing freestream Mach number. Also, both models can be made to achieve earlier activation of turbulence by increasing their freestream levels, but too high a level can disturb the turbulent solution behavior. The technique of maintaining freestream levels of turbulence without decay in the SST model, introduced elsewhere, is shown here to be useful in reducing grid-dependence of the model's transitional behavior. Both models are demonstrated to be incapable of predicting relaminarization; eddy viscosities remain weakly turbulent in accelerating or laterally-strained boundary layers for which experiment and direct simulations indicate turbulence suppression. The main conclusion is that these models are intended for fully turbulent high Reynolds number computations, and using them for transitional (e.g., low Reynolds number) or relaminarizing flows is not appropriate.

I. Introduction

The Spalart-Allmaras (SA) turbulence model[1] and the Menter k-ω shear-stress transport (SST) turbulence model[2] have been widely-used and trusted models for Reynolds-averaged Navier-Stokes (RANS) computations of aerodynamic flows for well over a decade. Recently, Rumsey[3] showed that, under certain circumstances, both of these models could exhibit inconsistent numerically-induced transition regions (near the stagnation region of airfoils) that vary with grid density. The problem with the SA model was easily solved by either using a freestream turbulence level higher than a particular threshold level or by making a simple change to one of the model constants. Spalart and Rumsey[4] subsequently determined the inconsistency in the SST model to be primarily due to grid-dependent decay rate of freestream turbulence for two-equation models. The authors also made general recommendations for effective inflow conditions for turbulence models, and showed how the addition of source terms in two-equation models can sustain the freestream ambient turbulence levels. This elimination of freesteam decay not only reduces the aforementioned problems associated with grid dependency, but it is also more representative of the physics inherent in both wind tunnel and flight.

Having achieved the ability to compute grid-consistent solutions, we now turn our attention to documenting the effects of Reynolds number and Mach number on the flowfields produced by these models. In particular, we focus on their inherent transitional behavior. It is important to recognize that, even when run in "fully-turbulent" mode, turbulence models do not necessarily yield a fully-turbulent solution everywhere in the boundary layer. There is often a region near the leading edge of aerodynamic bodies where the flow is effectively laminar because the eddy viscosity produced by the turbulence model is low. The low values of eddy viscosity are a consequence of the turbulence model not having sufficient turbulence-production strength from the mean shear flow; this capacity is a strong function of

*Senior Research Scientist, Computational Aerosciences Branch, Mail Stop 128, Associate Fellow AIAA.

†Boeing Senior Technical Fellow, Mail Stop 67-LM, Member AIAA.

the Reynolds number. The importance of checking computed results for unintended laminar behavior is sometimes stressed,[5] but in reality it is probably not done very often. When checking, the flow at a location is often considered turbulent when $\mu_t/\mu_\infty > 1$ in the boundary layer above the body surface, then the flow at that location is considered turbulent. Another criterion is the turbulence index i_t from Spalart and Allmaras,[1] which has a value close to zero in a laminar region and close to 1 in a turbulent region.

It is important to note that the SA and SST turbulence models – along with many other models in wide use today – were not designed to predict transition. They do not include any transition modeling capability or "tuning" per se. Thus, any transitional behavior exhibited by the models should not be expected to agree with real physical transition processes. This is one reason why Spalart and Rumsey made recommendations for freestream levels that were not based upon matching freestream turbulence (Tu) levels from wind tunnel or flight, but rather upon considerations related to preserving potential cores in small geometry features and maintaining the integrity of the turbulence quantities throughout the boundary layers. Nonetheless, there is some correspondence in the trends between the models and experiment: at lower Reynolds numbers the computed laminar regions can be quite extensive, while at higher Reynolds numbers the boundary layers go turbulent earlier. Users should be made aware that laminar flow regions may be occurring in their computations, especially at low or moderate Reynolds numbers. Very large regions of laminar flow may signify that the turbulence models are being utilized outside of their intended range of applicability. In other words, these turbulence models were intended for use in predicting turbulent flows; if the Reynolds number is so low that the flowfield is mostly laminar or transitional, then use of a transition model[6–12] would be more appropriate.

Because low Reynolds number flows are common for a wide variety of applications, including micro-air vehicles and many wind tunnel experiments, awareness of how the models behave in these circumstances, and guidance on whether they should even be used at all, can be critical. This paper seeks to document some of these characteristic behaviors of the SA and SST turbulence models. The goal is not to advocate using these models to predict transition (they should not!), but rather to demonstrate the kinds of transitional behaviors that can occur when using them in supposedly fully-turbulent simulations. To our knowledge this type of study has not been done before. It is hoped that this documentation will provide useful guidance for users *prior* to utilizing the SA or SST models for any particular application at low or moderate Reynolds number. We also investigate their ability to relaminarize in strongly accelerating boundary layer flows. Current applications are given for a flat plate and the NACA 0012 airfoil in both subsonic and supersonic flow conditions, and also for 2-D sink-flow and 3-D two-element infinite swept wing computations in subsonic conditions.

II. Numerical Method

The computer code CFL3D[13] solves the three-dimensional, time-dependent compressible RANS equations with an upwind finite-volume formulation (it can also be exercised in two-dimensional mode of operation for 2-D cases). Upwind-biased third-order spatial differencing is used for the inviscid terms, and viscous terms are centrally differenced. The code originally solved the thin-layer form of the equations (in each coordinate direction), but the full Navier-Stokes terms (i.e., cross-derivative terms) have recently been added. All solutions shown below use the full Navier-Stokes terms.

The CFL3D code is advanced in time with an implicit approximate factorization method. The implicit derivatives are written as spatially first-order accurate, which results in block tridiagonal inversions for each sweep. However, for solutions that utilize Roe flux-difference splitting,[14] the block tridiagonal inversions are further simplified using a diagonal algorithm with a spectral radius scaling of the viscous terms.

The turbulence models, including SA and SST, are solved uncoupled from the mean flow equations using implicit approximate factorization. Their advective terms can be solved using either first-order or second-order upwind differencing, with first-order the default for the code.

III. Turbulence Models

The one-equation SA model is written in terms of the turbulence quantity $\tilde{\nu}$.

$$\frac{\partial \tilde{\nu}}{\partial t} + u_j \frac{\partial \tilde{\nu}}{\partial x_j} = C_{b1}(1 - f_{t2})\tilde{S}\tilde{\nu} - \left[C_{w1} f_w - \frac{C_{b1}}{\kappa^2} f_{t2} \right] \left(\frac{\tilde{\nu}}{d} \right)^2 + \frac{1}{\sigma} \left[\frac{\partial}{\partial x_j} \left((\nu + \tilde{\nu}) \frac{\partial \tilde{\nu}}{\partial x_j} \right) + C_{b2} \frac{\partial \tilde{\nu}}{\partial x_i} \frac{\partial \tilde{\nu}}{\partial x_i} \right] \tag{1}$$

where a description of each of the terms is not given here, but can be found in the original reference.[1] The quantity $\tilde{\nu}$ is related to the eddy viscosity by:

$$\mu_t = \rho\tilde{\nu}\frac{(\frac{\tilde{\nu}}{\nu})^3}{(\frac{\tilde{\nu}}{\nu})^3 + c_{v1}^3} \tag{2}$$

where ν is the molecular kinematic viscosity and $c_{v1} = 7.1$.

The two-equation SST model is written in terms of the two turbulence quantities k and ω. When including the additional sustaining terms described in Spalart and Rumsey,[4] the form is:

$$\frac{Dk}{Dt} = \mathcal{P} - \beta^*\omega k + \frac{\partial}{\partial x_j}\left[\left(\nu + \frac{\nu_t}{\sigma_k}\right)\frac{\partial k}{\partial x_j}\right] + \beta^*\omega_{amb}k_{amb} \tag{3}$$

$$\frac{D\omega}{Dt} = \frac{\gamma}{\mu_t}\mathcal{P} - \beta\omega^2 + \frac{\partial}{\partial x_j}\left[\left(\nu + \frac{\nu_t}{\sigma_\omega}\right)\frac{\partial \omega}{\partial x_j}\right] + 2(1-F_1)\frac{1}{\sigma_{\omega 2}\omega}\frac{\partial k}{\partial x_j}\frac{\partial \omega}{\partial x_j} + \beta\omega_{amb}^2 \tag{4}$$

with $\mathcal{P} = \tau_{ij}\partial u_i/\partial x_j \approx \mu_t\Omega^2$ and Ω is the vorticity magnitude. The eddy viscosity is given by:

$$\mu_t = \rho\frac{a_1 k}{\max(a_1\omega, \Omega F_2)} \tag{5}$$

where $a_1 = 0.31$ and F_2 is a blending function. This model is identical to the original SST model in every respect except for the addition of constant sustaining terms $\beta^*\omega_{amb}k_{amb}$ and $\beta\omega_{amb}^2$. In the freestream, these have the effect of canceling the destruction terms if $k = k_{amb}$ and $\omega = \omega_{amb}$. Inside the boundary layer, they are generally orders of magnitude smaller than the destruction terms for reasonable freestream turbulence levels (say, Tu = 1% or less), and therefore have little effect. A complete description of each of the terms in the standard SST equations can be found in Menter.[2]

IV. Results

In Spalart and Rumsey,[4] the following recommendations were made for setting freestream turbulence levels. For the SA model: $\tilde{\nu}'_\infty = \tilde{\nu}_\infty/\nu_\infty = 3$. For k-ω models: $k_\infty/u_\infty^2 = 1\times10^{-6}$ and $\omega_\infty L/u_\infty = 5$. In coming up with these recommendations, consideration was given to gaps in multi-element configurations as well as to both well-developed and leading-edge boundary layers. Also, these recommended values rely on the assumption that freestream decay is being prevented in the two-equation models (freestream decay does not occur for $\tilde{\nu}$ in the SA model). Table 1 shows the correspondence between the recommended values and other commonly-referenced quantities and nondimensionalizations. Here, Tu (%) $= 100\sqrt{2/3(k_\infty/u_\infty^2)}$. For SA, $\mu_{t,\infty}/\mu_\infty = (\tilde{\nu}'_\infty)^4/[(\tilde{\nu}'_\infty)^3 + c_{v1}^3]$; for SST, $\mu_{t,\infty}/\mu_\infty = (k_\infty/u_\infty^2)/(\omega_\infty L/u_\infty)\mathrm{Re}$. Note that for the SA model, the freestream nondimensional eddy viscosity is near 0.21, whereas for SST (or other k-ω models) it varies depending on Reynolds number. For example, for $\mathrm{Re} = 100,000$: $\mu_{t,\infty}/\mu_\infty = 0.02$, for $\mathrm{Re} = 1\times10^6$: $\mu_{t,\infty}/\mu_\infty = 0.2$, and for $\mathrm{Re} = 1\times10^7$: $\mu_{t,\infty}/\mu_\infty = 2$.

Table 1. Correspondence between turbulence variables in the freestream

Model	$\tilde{\nu}_\infty/\nu_\infty$	k_∞/u_∞^2	$\omega_\infty L/u_\infty$	Tu (%)	$\mu_{t,\infty}/\mu_\infty$	k_∞/a_∞^2	$\omega_\infty\mu_\infty/(\rho_\infty a_\infty^2)$
SA	3	n/a	n/a	n/a	0.21044	n/a	n/a
SST	n/a	1×10^{-6}	5	0.08165	$(2\times10^{-7})\mathrm{Re}$	$(1\times10^{-6})M^2$	$5M^2/\mathrm{Re}$

A. Flat Plate

Two-dimensional zero-pressure-gradient flat plate computations were performed on a series of grids of size 273×193 (fine), 137×97 (medium), and 69×49 (coarse), with most of the runs on the medium grid. The grids extended over nondimensional distances $-0.33333 < x < 2$ and $0 < y < 1$. On the medium grid, the minimum grid spacing (wall normal direction) was 1×10^{-6}. This was fine enough to yield minimum y^+ levels well less than 0.1 at all conditions tested. The medium grid x-direction spacing was about 0.043, with clustering near the leading edge (x-spacing of 0.002) at $x = 0$. There were 25 points upstream of the plate leading edge and 113 points on the plate itself. The 3

grids were of the same family, so the fine and coarse grids had approximately double and half the medium grid spacing in both coordinate directions, respectively.

Boundary conditions were as follows. Symmetry conditions were imposed on the lower boundary faces located upstream of the leading edge at $x = 0$. On the plate, adiabatic solid wall conditions were imposed. The top boundary faces used farfield Riemann-type boundary conditions, and the downstream boundary used extrapolation. For subsonic flow, upstream faces used a characteristic method similar to the farfield Riemann method, except that total pressure and total temperature were set for the external state according to isentropic relations for the particular Mach number chosen. For supersonic flow, all inflow variables were specified.

The expected behavior for turbulence models for this type of flow is shown in figs. 1(a) and (b), which display contours of μ_t/μ_∞ for the SA and SST models at $M = 0.2$ and $\mathrm{Re}_L = 1 \times 10^6$, where L is unit 1 of the grid. (Recall that levels of $\mu_t/\mu_\infty > 1$ are typically considered turbulent). This is the expected typical behavior for turbulence models that are run "fully turbulent" (with no laminar regions imposed): turbulence initiates generally very near the leading edge. Velocity profiles in wall units at the fully-turbulent locations near $x = 0.5$ and 1.5 are shown in figs. 2(a) and (b), along with results the two models would give at very large Reynolds numbers.[a] Both models exhibit good comparisons with law-of-the-wall theory (with the particular choice of constants $\kappa = 0.41$, $B = 5.0$).[15]

Skin friction coefficients are shown in fig. 3, in comparison with the theoretical level given by $c_f = .025\mathrm{Re}_x^{(-1/7)}$. Downstream of the leading edge area, both models agree well with each other and with theory. For example, at $\mathrm{Re}_x = 1 \times 10^6$, both models are within about 0.3% of each other, and predict c_f about 1% low compared to theory. However, as is well-known, the turbulence models actually do not activate immediately at the leading edge, but rather at a finite distance downstream of the leading edge that varies with freestream conditions.

In order to explore the effect of Mach number on the location of turbulence model activation, computations were run at various Mach numbers ranging from $M = 0.2$ through $M = 7$. For $M \leq 2$, the Reynolds number used was $\mathrm{Re}_L = 100,000$ per unit length of the grid (or $\mathrm{Re} = 200,000$ over the entire plate). At higher M, it was necessary to run at higher Re_L in order to achieve activation on the plate.

Results showing the activation Re_x (the Re_x at which μ_t/μ_∞ first reaches 1) for $0.2 < M < 2.0$ for both models are given in fig. 4. The figure indicates that the SA model reaches $\mu_t/\mu_\infty = 1$ near $\mathrm{Re}_x = 20,000 - 25,000$ or so across this Mach number range, whereas SST goes turbulent somewhat later near $\mathrm{Re}_x = 40,000$ at $M = 0.2$ and near 60,000 at $M = 2.0$. Also shown in the figure are the effects of grid density, which tend to be somewhat greater for SST than for SA.

The behavior of skin friction in the "transition" region is shown in fig. 5, in this case at $M = 0.2$ (trends at other M are similar). The SA model exhibits a very gradual transition behavior from laminar to turbulent, approaching the turbulent theory curve from below. The SST model on the other hand exhibits a more "traditional" rapid transition behavior from laminar to turbulent, its skin friction overshooting the theory in the early stage, which is normal since the boundary layer is thinner. Further insight can be gained by looking at u^+ vs. y^+ plots shown in figs. 6(a) and (b). Both models show a very gradual approach toward turbulent log-layer behavior with increasing Re_x. Because SST yields a broader logarithmic overlap region than SA, it is difficult to compare the models directly in the region between $log(y^+) = 1$ and 1.5, but it appears that the SST model achieves self-similar behavior in this lower part of the log layer somewhat earlier. Similar trends are exhibited for $M = 2$, as shown in figs. 7(a) and (b).

We next explore differences in how the two models behave in this "transitional" region. Fig. 8(a) shows a plot of peak μ_t/μ_∞ for both models in the boundary layer at $M = 0.2$, for several freestream μ_t/μ_∞ levels. For the three highest freestream turbulence levels shown here, the SA model behaves consistently. (One of these is the recommended level from Spalart and Rumsey[4] of $\tilde{\nu}'_\infty = 3$ corresponding with $\mu_t/\mu_\infty = 0.21044$.) At the lowest freestream level of $\tilde{\nu}'_\infty = 0.517301$ corresponding with $\mu_t/\mu_\infty = 0.0002$, the SA model remains laminar in this case. This laminar behavior is probably due to the presence of the f_{t2} term in the model, which was designed to make $\tilde{\nu} = 0$ a solution to the equations with a small basin of attraction, so that numerical tripping could be delayed for transitional flows. The SST model exhibits greater overall influence by the freestream turbulence levels. Here, the middle SST curve has been generated using the recommended levels.[4]

Fig. 8(a) shows one aspect of the different behaviors of the models, but it fails to explain why SA does not exhibit the same type of laminar-to-turbulent transition as SST. Fig. 8(b) shows eddy viscosity profiles at three streamwise stations where each model achieved a peak of approximately $\mu_t/\mu_\infty = 0.2$, 1.0, and 8.0, respectively. In the region near the wall (below the peak), SA produces consistent levels even when peak μ_t/μ_∞ is very low. With these consistent levels, SA does not have low enough eddy viscosity to behave laminar; hence its c_f departs from laminar behavior quite early. SST, on the other hand, exhibits very different behavior. For the location where peak $\mu_t/\mu_\infty = 0.2$, its near wall eddy viscosity is much lower than it is at the downstream stations. Thus, SST behaves laminar upstream and

[a] Strelets, personal communication, 2006

produces a well-defined region of "transition" to turbulence.

In summary, the SA model exhibits the start of turbulence activation earlier than SST (in the sense that μ_t/μ_∞ reaches 1 within the boundary layer at a lower Re_x). Furthermore, SA's behavior near the wall causes its skin friction to appear transitional over a greater distance, whereas SST displays a well-defined laminar-to-turbulent trip behavior. In terms of log law behavior, both models gradually approach the correct slope, with SA perhaps taking slightly longer. However, these differences are probably not too important. The main point here is that for Mach numbers less than 2, both models behave laminar at very low $\mathrm{Re}_x < 20,000 - 60,000$ and then do not truly exhibit what might be considered turbulent behavior until $\mathrm{Re}_x > 100,000 - 300,000$ or so.

With the new ability to sustain freestream levels in the SST model as described in Section III, we can now investigate the effect of freestream levels of turbulence on the transitional behavior of the SST model with better transparency (without dependency on the grid size in the farfield). It is also possible to adjust the freestream level of $\tilde{\nu}$ in the SA model, corresponding to freestream μ_t/μ_∞. Results for the flat plate at $M = 0.2$ are shown in fig. 9(a) and (b). For the SA model, five values of freestream μ_t/μ_∞ were chosen. For SST, five values of freestream turbulence intensity (in percent) $\mathrm{Tu} = 100\sqrt{(2/3)k/u_\infty^2}$ were chosen. In all SST cases, $\omega L/u_\infty$ was held fixed at 5, so μ_t/μ_∞ varied as shown in the figure legend.

For SA, freestream $\tilde{\nu}'_\infty = 3$ corresponding with $\mu_t/\mu_\infty = 0.21044$ is the one recommended in Spalart and Rumsey.[4] The freestream value $k/u_\infty^2 = 1 \times 10^{-6}$, corresponding to $\mathrm{Tu} = 0.08165\%$, is the one recommended for SST. The SA model can be steered to yield laminar flow with very low values of freestream turbulence, in this example both $\mu_t/\mu_\infty = 0.0002$ and $\mu_t/\mu_\infty = 2 \times 10^{-6}$ yielded laminar flow. The SA model shows little difference for the next two higher freestream turbulence levels. As discussed earlier, because of the more gradual way that SA approaches fully turbulent behavior, it is difficult to designate a location where turbulence is actually achieved. For $\mu_t/\mu_\infty = 20$, the c_f is noticeably higher everywhere. For SST, the correct overall trend for transition to turbulence is exhibited: the higher the freestream Tu, the further forward the transition, although again at the highest Tu the downstream c_f levels are noticeably higher.

It should be stressed that the transition behavior shown in fig. 9(b) may or may not correspond quantitatively with experimentally-measured behavior. The SST model was certainly not designed to do so, and we are not trying to establish validity for transition predictions. However, it is reassuring to note that SST does exhibit the correct trend. This, then, seems to offer the user some level of control for achieving reduced regions of laminar flow when running at low Reynolds numbers. As discussed in Spalart and Rumsey, however, there are practical limits on freestream k/u_∞^2. If set too high (say, $\mathrm{Tu} > 1\%$), then the boundary layer levels may be influenced through diffusion, or the sustaining terms may become high compared to destruction terms in the boundary layer and affect the turbulence budget near the wall. This is likely the reason why the downstream skin friction for $\mu_t/\mu_\infty = 20$ is higher than the other three. Hence, there are practical limits to the ability to achieve turbulent flow at low Reynolds numbers with these models.

At Mach numbers higher than $M = 2$, both models have a greater tendency to remain laminar, with the SA model particularly reluctant to activate turbulence above approximately $M > 5$, as shown in fig. 10. For example, when using the recommended level of $\tilde{\nu}'_\infty = 3$ (corresponding with $\mu_t/\mu_\infty = 0.21044$) at $M = 6.4$, the SA model does not reach $\mu_t/\mu_\infty = 1$ until near $\mathrm{Re}_x = 1,172,000$. The SST model goes turbulent at this Mach number near $\mathrm{Re}_x = 400,000$. However, as noted above, by increasing $\tilde{\nu}'_\infty$ in the SA model, turbulence can be triggered earlier. An example is shown in the figure for $M = 6.4$ using $\tilde{\nu}'_\infty = 4.480729$ (corresponding with $\mu_t/\mu_\infty = 0.9$). In this case the SA model activates turbulence near $\mathrm{Re}_x = 400,000$.

Thus, for hypersonic Mach numbers, it may be more difficult to activate turbulence with these models, requiring either running at higher Reynolds numbers or employing higher freestream turbulence levels. Note, however, that the current forms of the turbulence models used here are incompressible, which are likely not accurate for many flows with high supersonic freestream Mach numbers.[16] There are compressible forms and/or corrections for these models (see for example Catris and Aupoix[17] and Wilcox[18]), but these were not tested here.

B. NACA 0012

A second set of test cases was run for the NACA 0012 airfoil, using a family of C-grids. The finest grid had 513×257 points, with 353 points on the airfoil surface, nondimensional chord length of $c = 1.0$, and minimum normal spacing at the wall of 6×10^{-7}. The farfield was located at $50c$. The medium grid (for which most runs were made) used every other point (257×129) with minimum normal spacing at the wall of 1.2×10^{-6}, and the coarse grid (129×65) was every other point of this. These minimum spacings yielded average minimum y^+ levels at the wall well less than 0.1 at all conditions tested.

Based on the earlier flat plate results, it is expected that computing flow over an airfoil at low Reynolds numbers of order $100,000$ will yield extensive regions of laminar flow over the forward part of the body. However, now the

"transition" of the turbulence models will also be influenced by streamwise adverse and favorable pressure gradients. Furthermore, because the farfield boundary is so far away in most external aerodynamic cases, it is expected that the capability to maintain freestream turbulence levels without decay in the SST model will be helpful in preserving consistency as the grid is refined.

The conditions run were $\mathrm{Re}_c = 100,000$ and $\alpha = 5^\circ$, over a range of Mach numbers. Example nondimensional eddy viscosity contours for the two turbulence models are shown in figs. 11(a) and (b) for $M = 0.2$. Values of μ_t/μ_∞ first exceed 1 at $x/c = 0.081$ (upper surface) and $x/c = 0.314$ (lower surface) for SA; and further aft at $x/c = 0.145$ (upper surface) and $x/c = 0.477$ (lower surface) for SST. Thus, as much as a third to a half of the lower surface in these cases is essentially laminar. In these figures, the shape of the NACA 0012 airfoil has been distorted to make it easier to visualize the extent of the turbulent regions.

As the freestream Mach number is increased, the turbulence activation locations on the airfoil tend to move further downstream. A summary plot is shown in fig. 12. Again, transition locations are based on the approximate locations where μ_t/μ_∞ first exceeds 1. The square symbols represent SA results, whose results go turbulent in the range of $0.3 < x/c < 0.4$ (lower surface) and $x/c = 0.1$ at low Mach numbers and $0.5 < x/c < 1$ for $M > 0.85$ (upper surface). The diamond symbols represent SST results, whose results go turbulent in the range of $0.5 < x/c < 0.75$ (lower surface) and $x/c = 0.15$ at low Mach numbers and $0.7 < x/c < 0.9$ for $M > 0.85$ (upper surface). It is interesting to note the fact that much of the upper surface very quickly loses turbulence at this Reynolds number between approximately $0.8 < M < 0.9$ for both models.

Grid resolution studies were conducted for all the cases at $M = 0.2$; these results are indicated on the left side of the figure. For SA, there was much less influence of grid on the location where $\mu_t/\mu_\infty = 1$ than there was for SST. Note also that when running SST and *allowing* decay of turbulence in the freestream, the dependence of turbulence activation on grid size is considerably greater, as indicated by the filled-in symbols. The reason for this increased dependence is the fact that turbulence decay rates in the farfield (where grid cells tend to be very large) are influenced by grid size changes. Hence, the local ambient turbulence level in the vicinity of the airfoil, which affects turbulence development in the boundary layer, depends on the grid. Removing this dependence by maintaining freestream turbulence levels yields more consistent results.

The behavior of the eddy viscosity in the freestream for the SST model with and without turbulence decay is shown in fig. 13, for $M = 0.2$. For comparison, the k-ε model free decay theory, given by:

$$\mu_t = \mu_{t,\infty} \left[1 + (C_{\varepsilon 2} - 1) \left(\frac{\varepsilon}{k} \right)_\infty \frac{x}{u_\infty} \right]^{\frac{C_{\varepsilon 2}-2}{C_{\varepsilon 2}-1}} \tag{6}$$

is also shown, where $C_{\varepsilon 2}$ is taken to be 1.92, $\omega L/u_\infty = 5$, and ω in the SST model is related to ε through the relation $\omega = \varepsilon/(0.09k)$. As discussed in Spalart and Rumsey,[4] real flow over external aerodynamic configurations has no reason to obey the decay equations used to calibrate two-equation models in isotropic turbulence. In reality, the kinetic energy (and eddy viscosity) relevant to the aircraft flow varies very little over the size of the typical CFD domain. Thus, the behavior represented by the non-decaying freestream turbulence is actually more representative of reality than the decaying behavior.

The bottom line of this airfoil study is that computing turbulent flow over airfoils at low Reynolds numbers can be problematic. Sometimes, experiments in wind tunnels are run at Reynolds numbers less than $\mathrm{Re}_c = 500,000$, and tripping is used to ensure turbulent flow. It is important to realize that computing such flows using turbulence models like SA or SST in "fully turbulent" mode will likely not achieve the same flow behavior. Rather, at low Re_c it is likely that the turbulence models will not become activated over much of the airfoil surface, and the higher the Mach number, the larger the laminar region is likely to be.

C. 2-D Sink-Flow and 3-D Infinite Swept Wing Flow

Having explored the behaviors of the SA and SST models at low Reynolds numbers from laminar to turbulent states, we now turn to the question of whether or not the models are capable of predicting relaminarization. This study was done by computing both 2-D sink-flow as well as a 3-D infinite swept two-element wing.

Sink-flow has been examined extensively both in experiments and computations. See, for example, Jones and Launder[19] and Spalart.[20] Here the sink-flow was computed on a grid of size 257×97 between two converging plates. At inflow ($x/L = 0$), the plates were separated a nondimensional distance of $y/L = 3.6265$ and at outflow ($x/L = 20$) they were separated by $y/L = 0.1$ (i.e., the top plate converged toward the lower at an angle of 10°). Minimum spacing at the walls was $\Delta y/L = 1.8 \times 10^{-4}$ at inflow and 5.0×10^{-6} at outflow, which was small enough to yield an average minimum $y^+ < 0.5$ for all cases computed. At inflow, a turbulent-like velocity profile was specified

along with appropriate approximated turbulence variable properties, with bulk $M = 0.01$ and pressure extrapolated from the interior. Density at inflow was set to its reference condition. At the outflow, pressure was set at $p/p_{\rm ref} = 1.0$ and all other quantities were extrapolated from the interior. This procedure set up an accelerating flow that developed to a nearly self-similar state over approximately the last half of the channel, with near-constant skin friction coefficient based on edge conditions, and sustained streamwise acceleration parameter K_s:

$$K_s = \frac{\nu}{U_e^2}\frac{dU_e}{dx} \tag{7}$$

where U_e is the velocity at the edge of the boundary layer. Different values for K_s were achieved by specifying different Reynolds numbers (effectively varying ν). A plot of $c_{f,Ue}$ along the wall for three different K_s is given in fig. 14. After the flowfield sets up, it is seen to achieve roughly constant $c_{f,Ue}$ for approximately $10 < x/L < 18$. Over this range, the edge velocity quadruples. The values of K_s were chosen to bracket the critical value of $K_s \approx 3 \times 10^{-6}$ at and above which relaminarization is considered likely,[20] and also included a value double the critical value. The $c_{f,Ue}$ achieved for $K_s = 2\times10^{-6}$ in the self-similar region agrees fairly well with the turbulent value of approximately $c_{f,Ue} = 0.0046$ measured at the same K_s by Jones and Launder.[19]

Fig. 15(a) and (b) shows normalized turbulent shear stress profiles ($-\overline{u'v'}/U_e^2$) within the self-similar region for both SA and SST using three different K_s values. Both models show a slight decrease in peak $-\overline{u'v'}$ as K_s is increased, with SA decreasing slightly more than SST. The data was extracted from 3 different x-locations in the channel to demonstrate that nearly self-similar behavior has been achieved (more so for SA than for SST). Jones and Launder[19] noted that $-\overline{u'v'}/U_e^2$ should dramatically decrease as K_s increases near these levels, and Spalart[20] showed that DNS computations near $K_s = 3 \times 10^{-6}$ became laminar. However, the current computations maintain turbulence even as high as $K_s = 6 \times 10^{-6}$, and do not predict the expected decrease. An example plot shows eddy viscosity for the SST model with $K_s = 6 \times 10^{-6}$ in fig. 16; it is seen to continuously increase in the boundary layer throughout the accelerating flowfield. The SA models yields similar results. In other words, neither SA nor SST shows evidence of relaminarization.

For the infinite swept wing, we employed the NLR 7301 wing section and used the experimental data of Viswanath et al.[21] as a guide. The NLR 7301 airfoil section (with a main element and flap) has been widely used in 2-D studies. See Rumsey and Ying[22] for a summary. In Viswanath et al., a wing with 45° sweep was built from this section, and an effort was made to approximate infinite sweep conditions by using a reasonably large span and end plates to avoid tip effects. Conditions were ${\rm Re}_c = 1.3 \times 10^6$, $M \approx 0.14$, and the model angle of attack was varied from 0° to 18°.

The CFD was carried out on two grids with farfield extent of approximately $50c$, and spanwise extent of $0.1c$ (with 45° sweep included), and periodic boundary conditions. The fine grid had 2.74 million cells with minimum spacing at walls of $3 \times 10^{-6}c$ and 16 spanwise cells. There were 481 chord-wise planar gridpoints on the main element surface and 449 on the flap surface. The coarse grid used every other point from the fine grid. For both grids the average minimum y^+ at the body was less than 1. A 2-D plane of the multi-zone fine grid is shown in fig. 17.

In the experiment, surface flow visualization revealed a laminar separation bubble on the upper surface near the nose of the main element for all angles of attack $\alpha > 3^\circ$, even though the attachment line was turbulent. Computations were performed here for $\alpha = 6^\circ$. At much higher angles of attack, significant trailing edge flow separation occurred, inhibiting convergence. Typical surface streamtraces from the computations are shown in fig. 18. Flow is from left to right. The flow attachment line (not seen) is on the lower surface of the main element near $x/c = 0.05$, and flow turning near the main element trailing edge can be seen. At these conditions the flow separates near the upper surface trailing edge of the flap.

The attachment line Reynolds number, $\bar{R} = Q_\infty \sin\Lambda(\eta^*/\nu)$ for these conditions in the experiment is between 200 and 250. Here, Q_∞ is the freestream total velocity, Λ is the sweep angle and $\eta^* = \sqrt{\nu/(\partial U_e/\partial n)}$, where U_e is the inviscid edge velocity component in the $+n$ direction and n is the direction normal to the wing leading edge in the downstream direction. This level is lower than the critical $\bar{R} = 250$ above which the attachment line is known to sustain turbulence in experiments, flight,[23–25] and direct numerical simulation (DNS).[26] However, our own computation from the CFD result yielded $\bar{R} = 305$. Its calculation is rather sensitive, and our attachment line has migrated to a region with weak surface curvature. Both turbulence models produced peak eddy viscosity levels in the vicinity of the leading edge that were slightly greater than 1, and the flow remained turbulent (although weakly) everywhere downstream on the main element. Even though the skin friction is not greatly affected locally, the eddy viscosity grows again after the pressure gradient reverses from favorable to adverse, thus preventing laminar separation.

A parameter proposed by Viswanath et al.[21] to determine if relaminarization is likely in this 3D flow is a generalization of the local streamwise acceleration parameter, K_s (eq. (7)):

$$K_s = \frac{\nu}{Q_e^2}\frac{\partial U_e}{\partial n}\cos^2\psi_e \tag{8}$$

where Q_e is the local edge total velocity and ψ_e is the angle between the local inviscid streamline and the $+n$ direction. We believe a more logical generalization from 2D to 3D would be

$$K_s = \frac{\nu}{Q_e^2}\frac{\partial Q_e}{\partial n}\cos\psi_e, \tag{9}$$

but in an infinite swept flow, the two are equivalent due to the relationship $Q_e \sin\psi_e = Q_\infty \sin\Lambda = U_e \tan\psi_e$.

When K_s sustains values above 3×10^{-6}, relaminarization is likely.[21,23,26] In Viswanath et al., at higher angles of attack of 15° and 17°, the peak K_s was nearly 1×10^{-5}. In the current computations at $\alpha = 6^\circ$, the peak K_s was even higher: more than 2×10^{-5}, as shown in fig. 19. Note that the computation of K_s can be difficult because it involves gradients of the somewhat difficult-to-determine edge value U_e (or Q_e). For low Mach numbers, one can estimate Q_e from $Q_e = Q_\infty\sqrt{1-c_p}$ and $\cos\psi_e$ from $\cos\psi_e = \sqrt{1-[\sin^2\Lambda/(1-c_p)]}$; in this case, using eq. (9), the peak K_s only differs from that computed with the method of finding appropriate edge values (by estimating their grid index location) by about 10%. Thus, both CFD and experiment strongly indicate that relaminarization is likely in this case.

However, neither the SA nor the SST turbulence model indicates any tendency toward relaminarization. As indicated in fig. 19, which shows results for both models on two different grids, the peak eddy viscosity in the upper surface boundary layer remains well above 1. Surface skin friction coefficients (fig. 20) also indicate no tendency toward any sort of laminar separation bubble, which occurred near $x/c = 0.05$ in the experiment. Although not shown, we also ran cases at half the Reynolds number, for which $\bar{R}$ is appreciably less than 250. In these cases, the peak eddy viscosity in the boundary layer is lower, as expected, but it grows nonetheless and prevents laminar separation. The perfect RANS model would sustain the attachment line turbulence if $\bar{R} > 250$, even with zero ambient value (but not zero initial value), and stop sustaining as soon as $\bar{R}$ drops below 250. Here, the models incorrectly sustain turbulence even with low $\bar{R}$, just like they did with high K_s in the sink flow. Another test of SA which is not shown was to drop the freestream eddy viscosity to zero, after convergence with the usual value; it made no appreciable difference in the solution. This swept-wing behavior therefore markedly differs from the 2D behavior in fig. 8(a).

This inability to predict laminar separation means that in practice one would need to manually "turn off" these models in the nose region in order to see any kind of bubble develop. The Baldwin-Lomax model[27] has precisely this feature of turning off eddy viscosity when the peak across the boundary layer is less than 14 times the freestream molecular viscosity, but a primary requirement in modern turbulence models is to have a local formulation, so that such a peak value is not a candidate for modification.

V. Conclusions

In conclusion, the SA and SST turbulence models – when run "fully turbulent" for high Reynolds number aerodynamic flows (typically on the order of $\mathrm{Re}_L = 1 \times 10^6$ or greater where L is the relevant geometric length scale of the body or wing) – usually yield turbulent fields with only relatively small regions near stagnation points where eddy viscosity is too low to produce typical turbulent behavior. When these regions are small, they generally do not have much of an effect on the global flowfield. However, when run at lower Reynolds numbers, the models' laminar or not-fully-turbulent extent can become significant compared to the geometric reference length. For zero pressure gradient flat plate flow, the SA model first yields $\mu_t/\mu_\infty > 1$ near $\mathrm{Re}_x = 20,000$ for $0.2 < M < 2.0$. The SST model transitions somewhat later, near $\mathrm{Re}_x = 40,000$ for $M = 0.2$ and near $\mathrm{Re}_x = 60,000$ for $M = 2.0$. The SA model generally yields higher eddy viscosity levels in the boundary layer leading up to transition compared to SST. As a result, SA's skin friction shows more transitional behavior in the region where $\mu_t/\mu_\infty < 1$. Note that there is no absolute target behavior here, because natural transition is far from unique in reality. At higher supersonic Mach numbers, both turbulence models have a greater tendency to remain laminar, especially the SA model using the recommended freestream value of $\tilde{\nu}'_\infty = 3$. For $M > 5$ it appears to be necessary to increase its freestream $\tilde{\nu}'_\infty$ to about 5 in order to activate turbulence at a reasonable Re_x.

Airfoil flow has been shown to behave similarly by computing a series of examples at low $\mathrm{Re}_c = 100,000$. Transition in these cases occurred between 10% c and the trailing edge (i.e., not at all), depending on the freestream Mach number. Again, as the Mach number is increased, airfoil flow shows a greater tendency for laminar boundary layer behavior for both models at low Reynolds number.

The technique of maintaining freestream levels of turbulence without decay by way of "sustaining terms" in the SST model has proved to be useful in reducing grid-dependence of the model's transitional behavior. Eliminating

freestream decay is also more physically realistic for external aerodynamic problems and – because it is the *local* levels of ambient turbulence that determine the turbulent behavior in the boundary layer – eliminating freestream decay makes it easier to understand and control the model's behavior. The SA model does not face this same issue; it is already designed so that its freestream level does not decay.

Also, flows with relaminarization are not predicted correctly with the SA or SST turbulence models. Eddy viscosities remain turbulent in accelerating or laterally-strained boundary layers for which experiment and direct simulations indicate turbulence suppression. The lesson to be learned from this study is that care should be exercised when using turbulence models for relaminarizing flows or flows at transitional Reynolds numbers. In these cases the turbulence models are operating outside of the range of applicability their authors have been able to address, and the flowfield physics are not likely to be predicted accurately. Although strong turbulent skin friction downstream usually limits the importance of the leading edge region, in rare instances missing the physics in this area will prevent the models from predicting a separation which would influence the entire flow-field.

References

[1]Spalart, P. R., and Allmaras, S. R., "A One-Equation Turbulence Model for Aerodynamic Flows," *La Recherche Aerospatiale*, No. 1, 1994, pp. 5–21.

[2]Menter, F. R., "Two-Equation Eddy-Viscosity Turbulence Models for Engineering Applications," *AIAA Journal*, Vol. 32, No. 8, 1994, pp. 1598–1605.

[3]Rumsey, C. L., "Apparent Transition Behavior of Widely-Used Turbulence Models," *International Journal of Heat and Fluid Flow* (to be published), 2007.

[4]Spalart, P. R. and Rumsey, C. L., "Effective Inflow Conditions for Turbulence Models in Aerodynamic Calculations," *AIAA Journal*, Vol. 45, No. 10, 2007, pp. 2544–2553.

[5]Rumsey, C. L. and Biedron, R. T., "Computation of Flow Over a Drag Prediction Workshop Wing/Body Transport Configuration Using CFL3D," NASA/TM-2001-211262, December 2001.

[6]D. C. Wilcox, "Simulation of Transition with a Two-Equation Turbulence Model," AIAA J. **32**, No. 2, 247–255 (1994).

[7]D. K. Walters and J. H. Leylek, "A New Model for Boundary Layer Transition Using a Single-Point RANS Approach," ASME J. Turbomachinery **126**, 193–202 (2004).

[8]C. Wang and B. Perot, "Prediction of Turbulent Transition in Boundary Layers Using the Turbulent Potential Model," J. Turbulence **3**, 22–36 (2004).

[9]Y. B. Suzen and P. G. Huang, "Modeling of Flow Transition Using an Intermittency Transport Equation," ASME J. Fluid Eng. **122**, 273–284 (2000).

[10]E. S. Warren and H. A. Hassan, "Transition Closure Model for Predicting Transition Onset," J. Aircraft **35**, No. 5, 769–775 (1998).

[11]F. R. Menter, R. B. Langtry, S. R. Likki, Y. B. Suzen, P. G. Huang, S. Volker, "A Correlation-Based Transition Model Using Local Variables, Part 1 - Model Formulation," Paper GT2004-53452, Proceedings of ASME Turbo Expo 2004, June 14-17, Vienna, Austria (2004).

[12]D. Marinov and Z. Zapryanov, "Numerical Modelling of Laminar-Turbulent Transition in the Boundary Layers Under the Influence of Low Free-Stream Turbulence Intensities," Comput. Meth. in Applied Mech. & Eng. **110**, 263–273 (1993).

[13]Krist, S. L., Biedron, R. T., and Rumsey, C. L., "CFL3D User's Manual (Version 5.0)," NASA TM-1998-208444, June 1998.

[14]Roe, P. L., "Approximate Riemann Solvers, Parameter Vectors, and Difference Schemes," *J. Comp. Phys.*, Vol. 43, 1981, pp. 357–372.

[15]White, F. M., *Viscous Fluid Flow*, McGraw-Hill Book Company, New York, 1974, p. 475.

[16]Gatski, T. B., Rumsey, C. L., and Manceau, R., "Current Trends in Modelling Research for Turbulent Aerodynamic Flows," *Philosophical Transactions of the Royal Society A*, Vol. 365, 2007, pp. 2389–2418.

[17]Catris, S. and Aupoix, B., "Density Corrections for Turbulence Models," *Aerospace Science and Technology*, Vol. 4, 2000, pp. 1–11.

[18]Wilcox, D. C., *Turbulence Modeling for CFD*, 3rd edition, DCW Industries, Inc., La Canada, CA, 2006.

[19]Jones, W. P. and Launder, B. E., "Some Properties of Sink-Flow Turbulent Boundary Layers," *Journal of Fluid Mechanics*, Vol. 56, part 2, 1972, pp. 337–351.

[20]Spalart, P. R., "Numerical Study of Sink-Flow Boundary Layers," *Journal of Fluid Mechanics*, Vol. 172, 1986, pp. 307–328.

[21]Viswanath, P. R., Mukund, R., Narasimha. R., and Crouch, J. D., "Relaminarization on Swept Leading Edges Under High-Lift Conditions," *AIAA Journal*, Vol. 44, No. 11, 2006, pp. 2621–2629.

[22]Rumsey, C. L. and Ying, S. X., "Prediction of High Lift: Review of Present CFD Capability," *Progress in Aerospace Sciences*, Vol. 38, 2002, pp. 145–180.

[23]Van Dam, C. P., Vijgen, P. M. H. W., Yip, L. P., and Potter, R. C., "Leading-Edge Transition and Relaminarization Phenomena on a Subsonic High-Lift System," AIAA Paper 93-3140, 1993.

[24]Poll, D. I. A., "Transition in the Infinite Swept Attachment Line Boundary Layer," *Aeronautical Quarterly*, Vol. 30, part 4, Nov. 1979, pp. 607–629.

[25]Arnal, D. and Juillen, J. C., "Leading-Edge Contamination and Relaminarization on a Swept Wing at Incidence," *Numerical and Physical Aspects of Aerodynamic Flows IV*, Ed: T. Cebeci, Springer-Verlag, Berlin, 1990, pp. 391–402.

[26]Spalart, P. R., "Direct Numerical Study of Leading-Edge Contamination," AGARD Symposium on Fluid Dynamics of 3D Turbulent Shear Flows and Transition, AGARD-CP-438, Oct. 3-6 1988, Turkey.

[27]Baldwin, B. S. and Lomax, H., "Thin Layer Approximation and Algebraic Model for Separated Turbulent Flows, AIAA Paper 78-257, 1978.

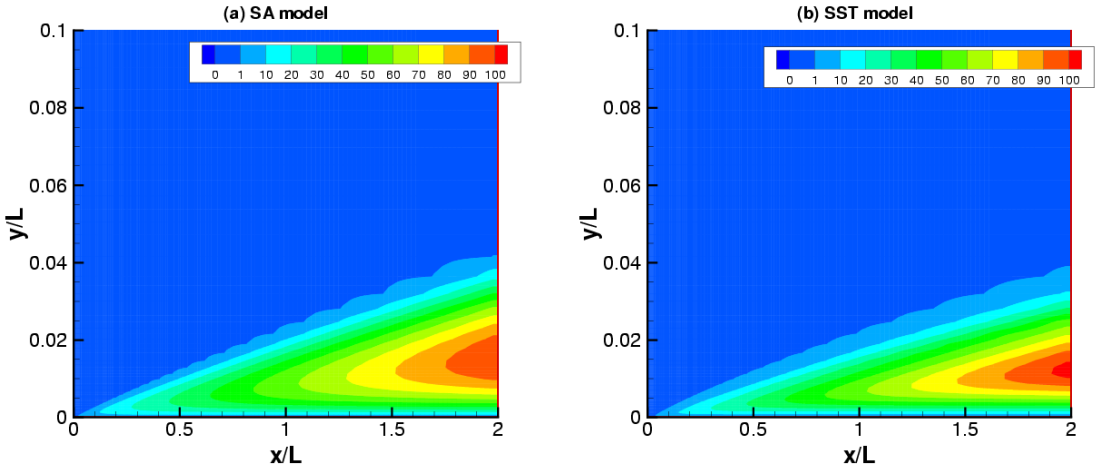

Figure 1. Contours of μ_t/μ_∞ for subsonic flow over flat plate, $M = 0.2$, $\mathrm{Re}_L = 1 \times 10^6$, medium grid.

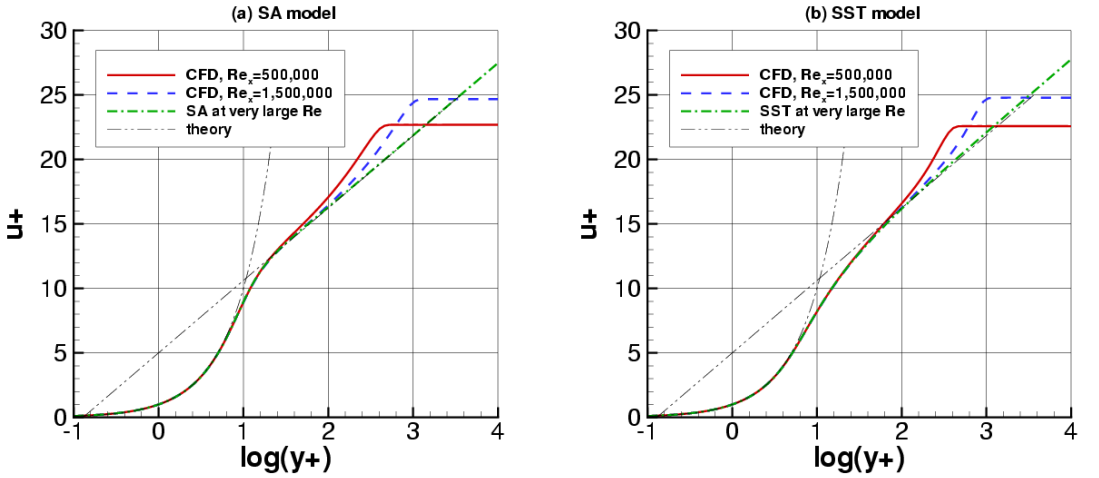

Figure 2. Velocity profiles in wall units for subsonic flow over flat plate, $M = 0.2$, $\mathrm{Re}_L = 1 \times 10^6$, medium grid.

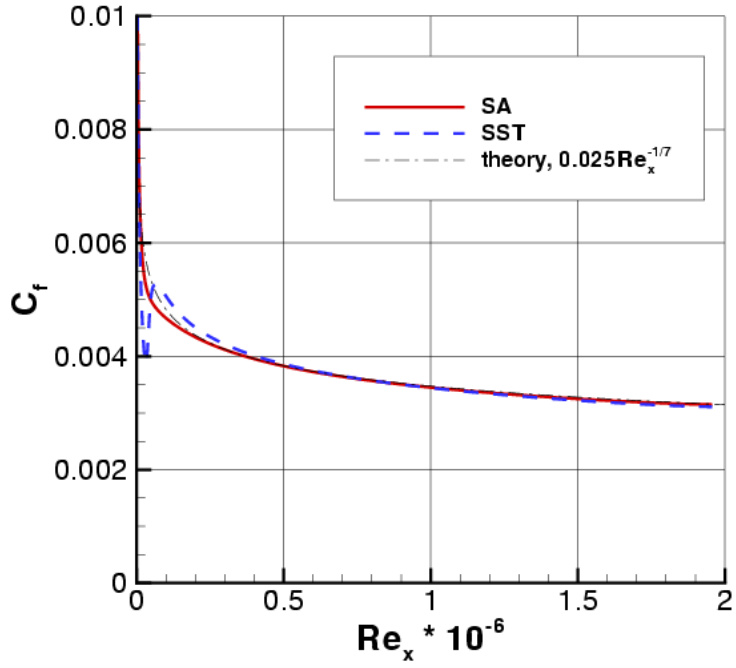

Figure 3. Skin friction coefficients for subsonic flow over flat plate, $M = 0.2$, $\mathrm{Re}_L = 1 \times 10^6$, medium grid.

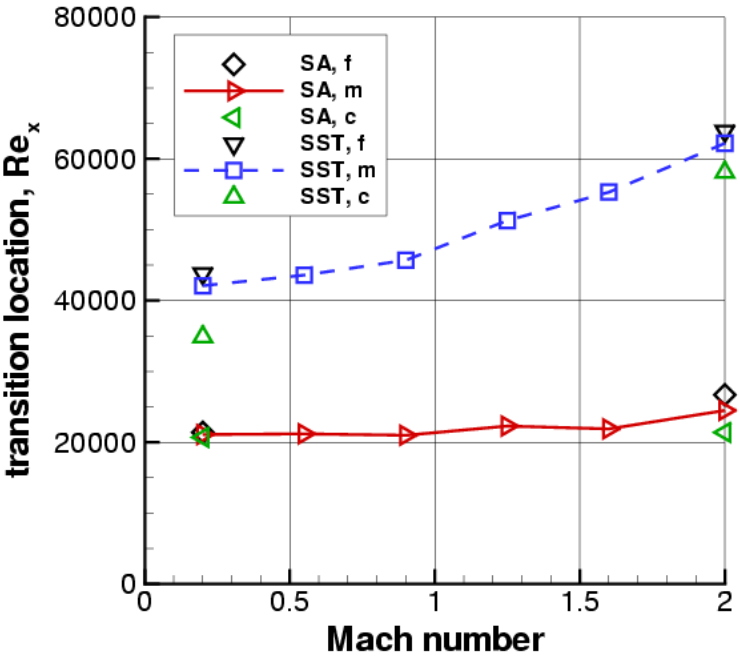

Figure 4. Flat plate Re_x location where models go turbulent (defined by $\mu_t/\mu_\infty \geq 1$), including effect of grid density (c=coarse grid, m=medium grid, f=fine grid).

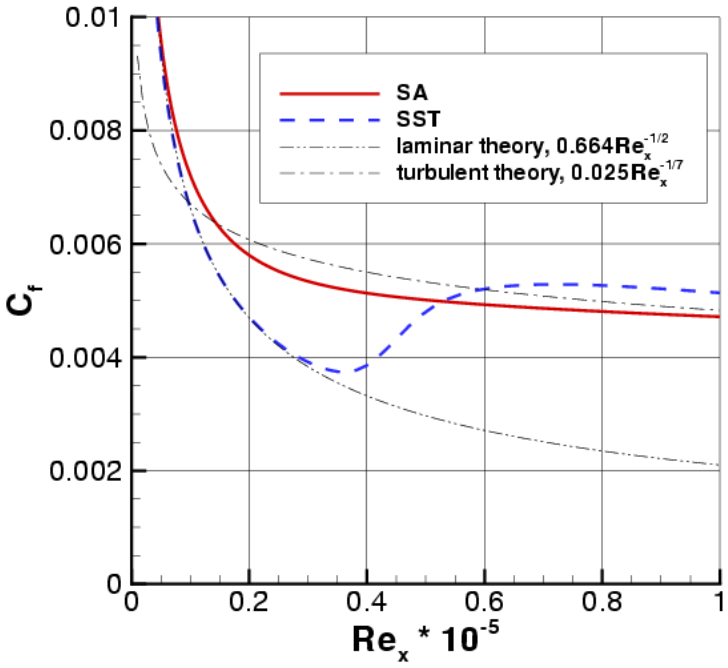

Figure 5. Transitional behavior of the models: skin friction coefficient on medium grid at $M = 0.2$.

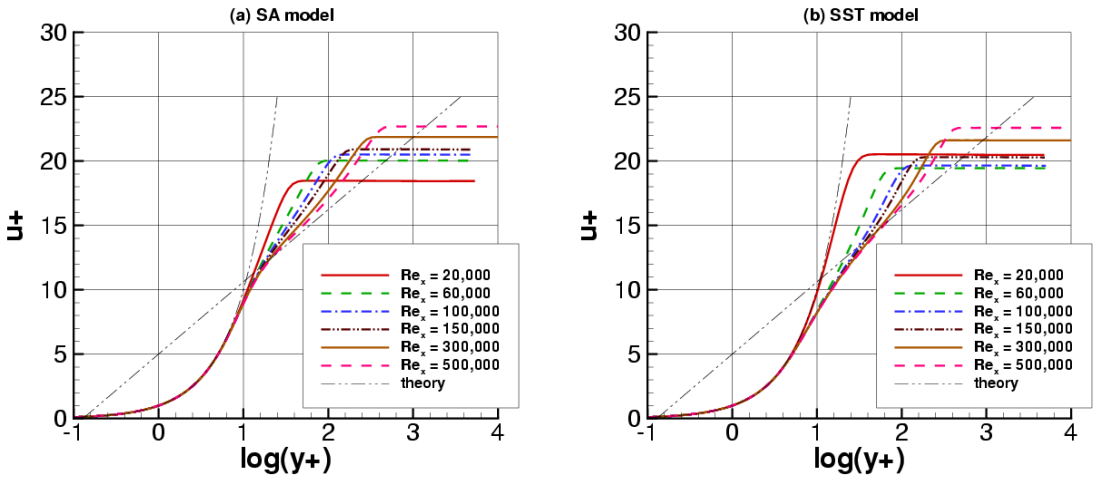

Figure 6. Velocity profiles in wall units in transitional region over flat plate, $M = 0.2$, medium grid.

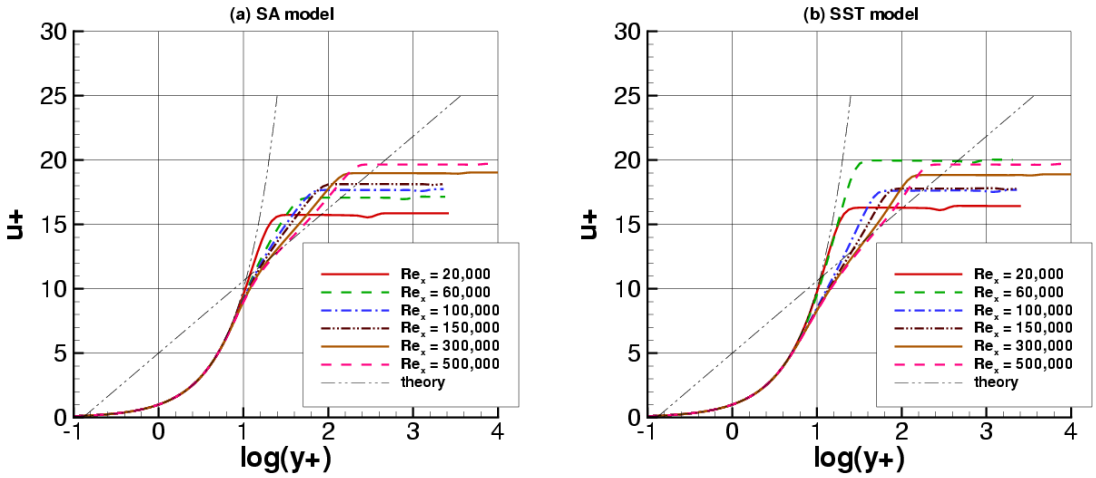

Figure 7. Velocity profiles in wall units in transitional region over flat plate, $M = 2.0$, medium grid.

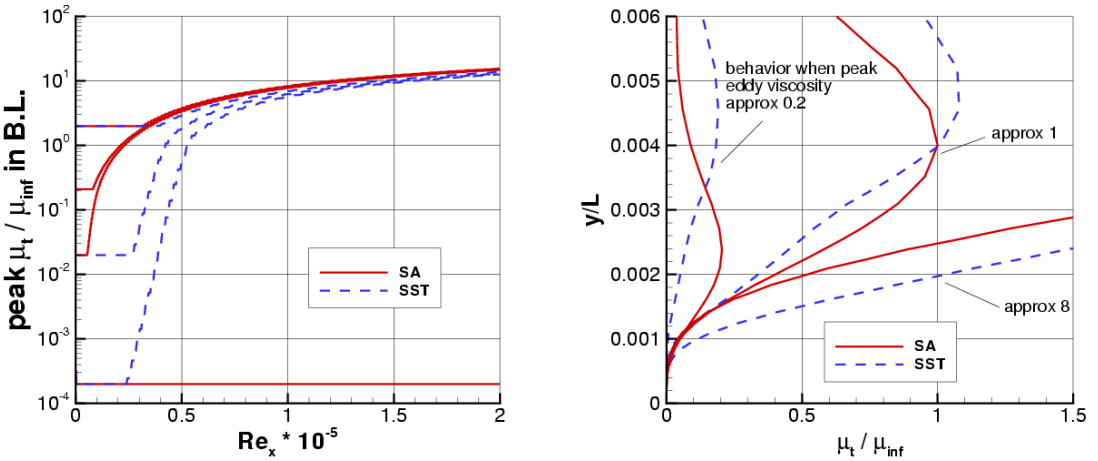

Figure 8. Eddy viscosity over flat plate, $M = 0.2$, medium grid; (a) peak value; (b) vertical profile at locations where peak $\mu_t/\mu_\infty \approx 0.2$, 1.0, and 8.0.

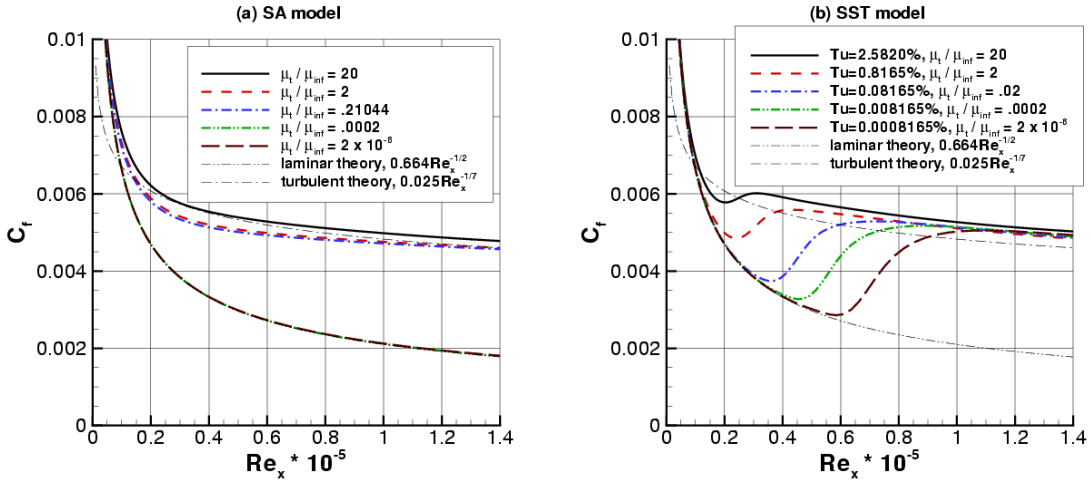

Figure 9. Skin friction coefficients for subsonic flow over flat plate showing effect of freestream μ_t/μ_∞ and Tu, $M = 0.2$, medium grid (blue dash-dot lines correspond with recommended freestream levels from Spalart and Rumsey[4]).

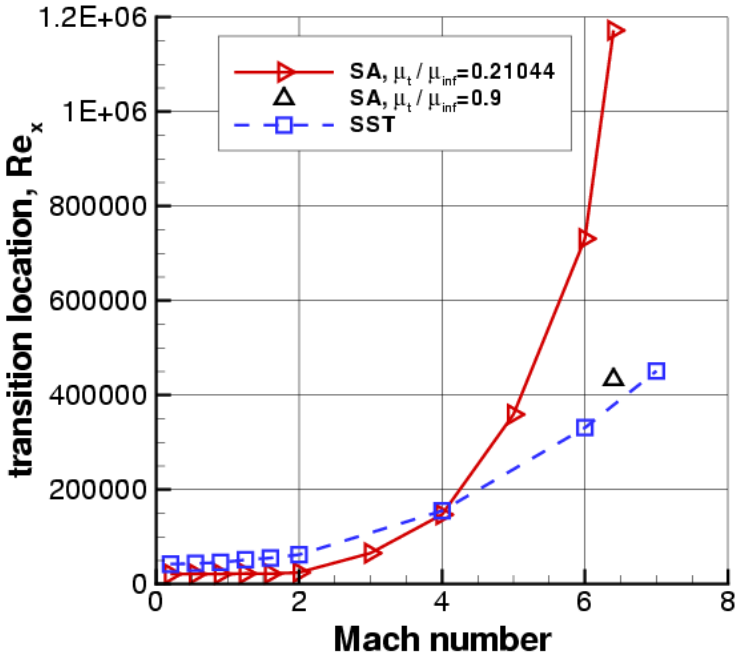

Figure 10. Re_x location where models go turbulent (defined by $\mu_t/\mu_\infty \geq 1$) for flat plate at higher Mach numbers, medium grid.

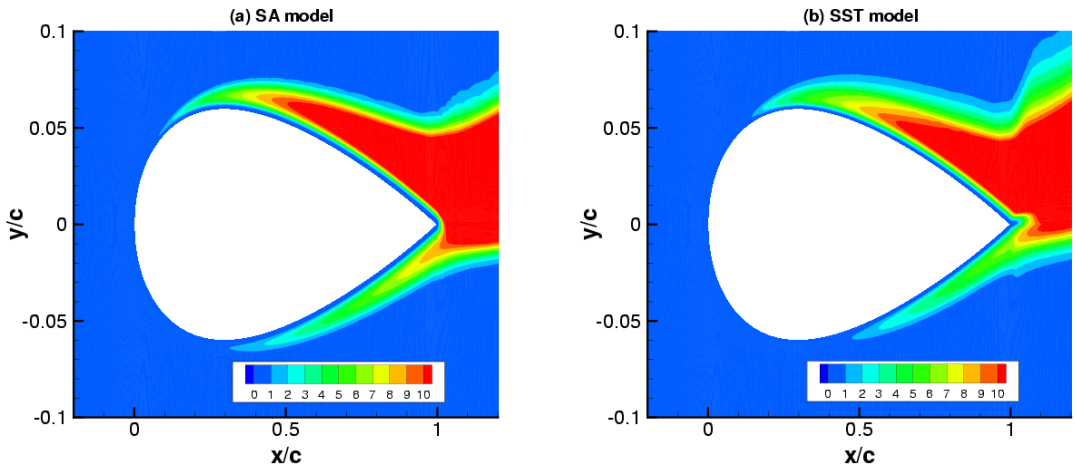

Figure 11. Contours of μ_t/μ_∞ for flow over NACA 0012 airfoil, $M = 0.2$, $\alpha = 5°$, $\mathrm{Re}_c = 100,000$, medium grid.

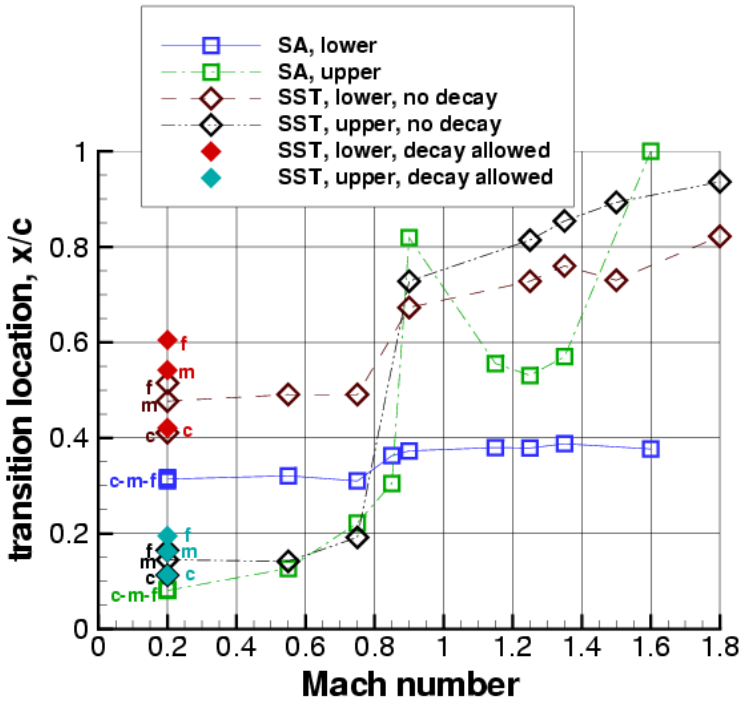

Figure 12. NACA 0012 airfoil x/c location where models go turbulent (defined by $\mu_t/\mu_\infty \geq 1$) for $\mathrm{Re}_c = 100,000$, $\alpha = 5°$, including effect of grid density at $M = 0.2$.

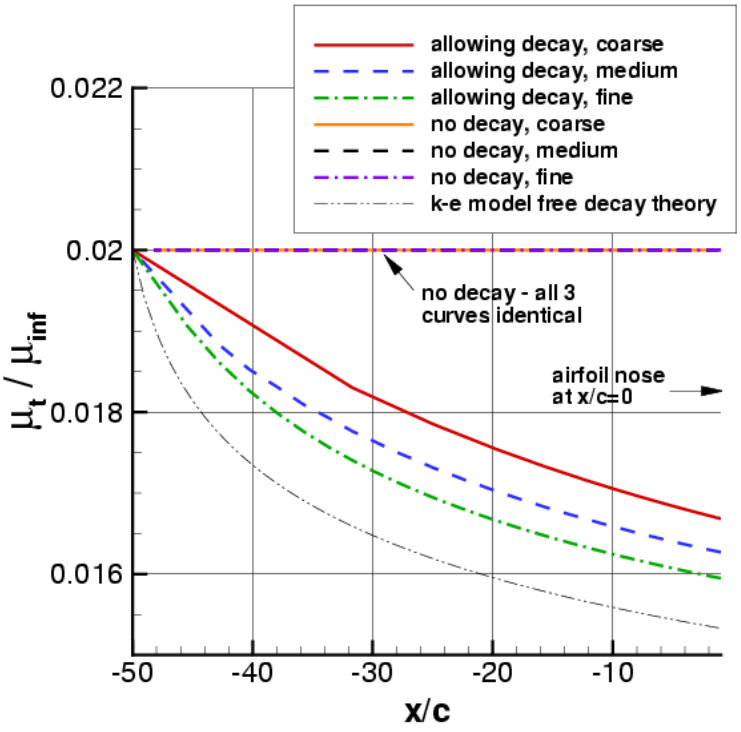

Figure 13. Behavior of SST freestream μ_t/μ_∞ over the $50c$ from inflow boundary to the vicinity of the airfoil as a function of grid density, $M = 0.2$.

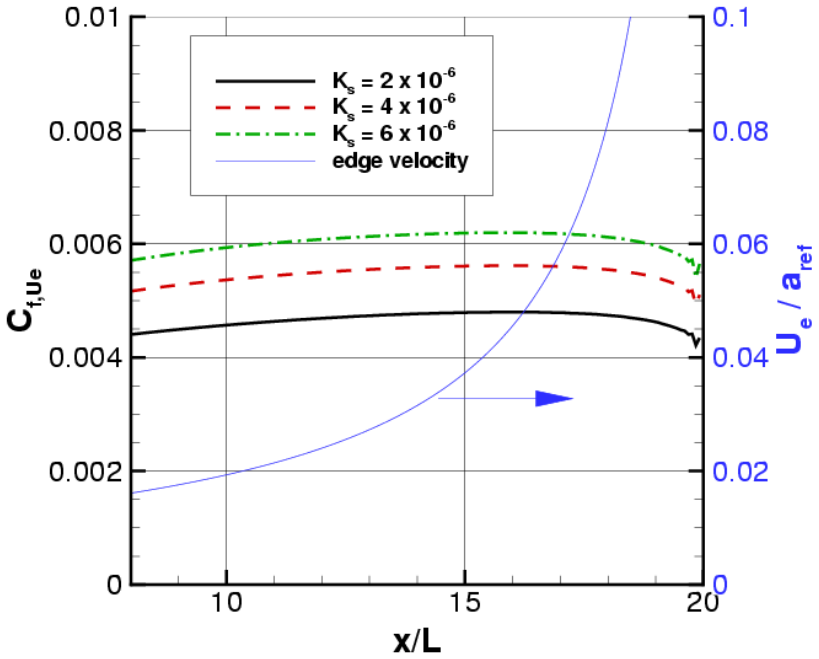

Figure 14. Skin friction coefficients for 2-D sink-flow at three different streamwise acceleration parameters using SST model, along with computed edge velocity.

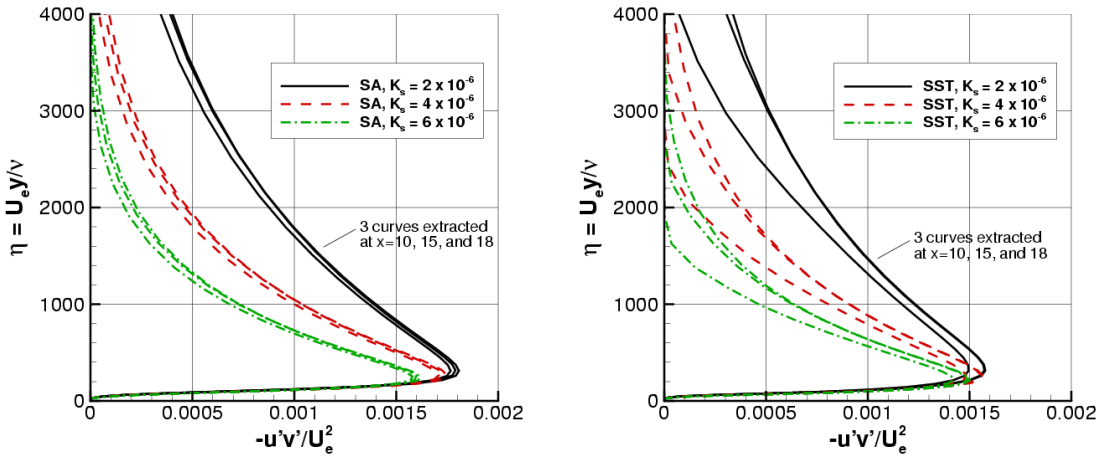

Figure 15. Turbulent shear stress profiles for SA and SST for 2-D sink-flow at three different streamwise acceleration parameters.

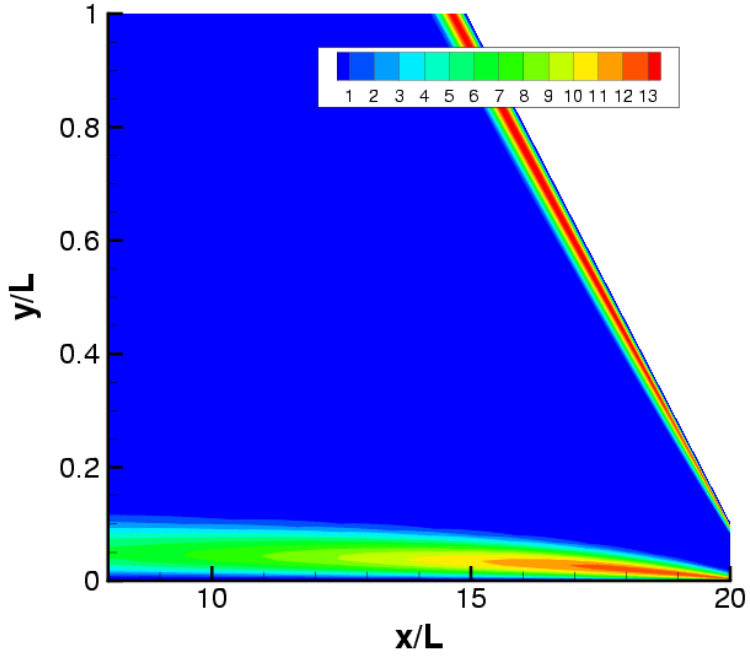

Figure 16. Contours of μ_t/μ_∞ for sink-flow, SST model, $K_s = 6 \times 10^{-6}$ (flow is from left to right, and view is expanded in y-direction for clarity).

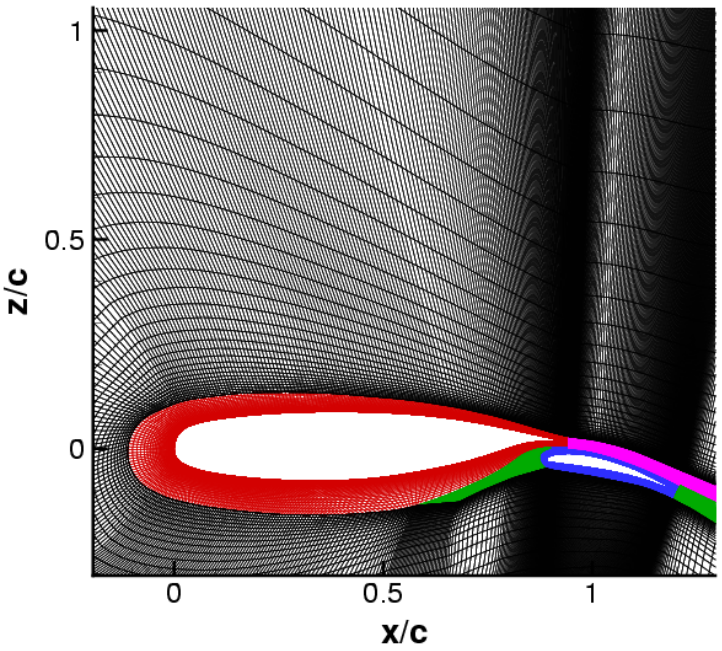

Figure 17. 2-D plane of NLR 7301 grid used for infinite swept wing computations.

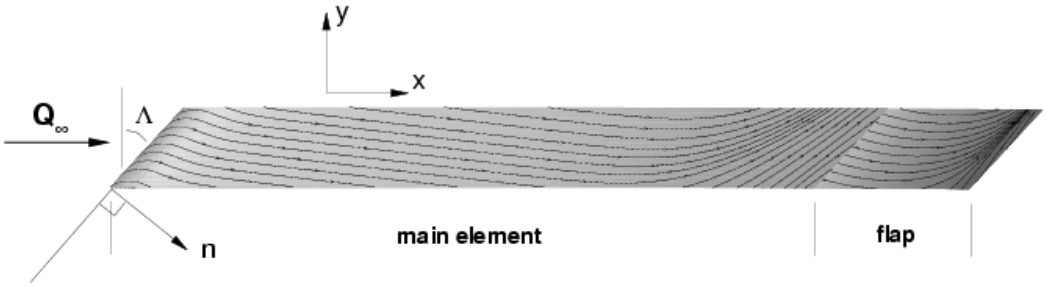

Figure 18. Example surface streamtraces for NLR 7301 infinite swept wing computation, $\mathrm{Re}_c = 1.3 \times 10^6$**,** $M = 0.14$**,** $\alpha = 6°$**,** $\Lambda = 45°$**.**

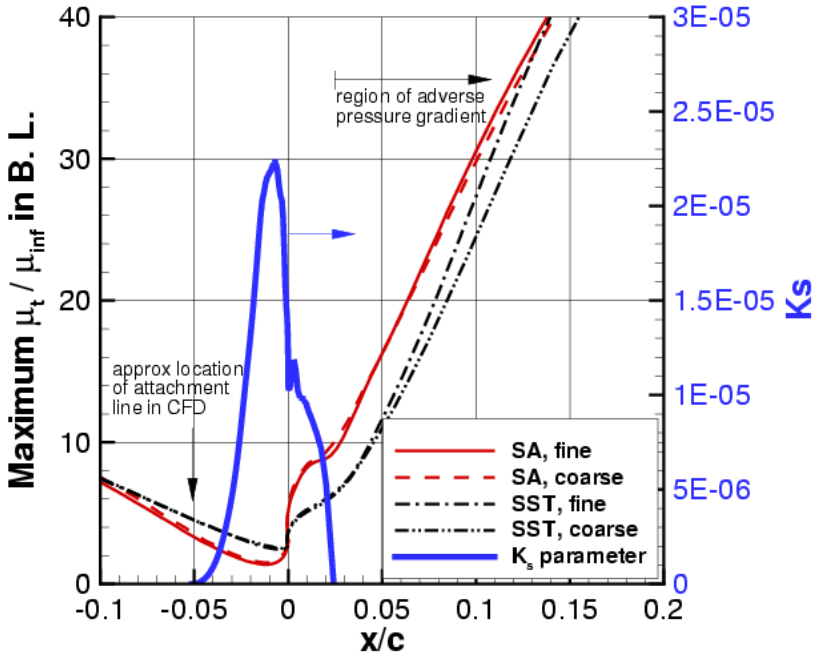

Figure 19. Plot of K_s and peak μ_t/μ_∞ in the boundary layer for the main element of the NLR 7301 infinite swept wing, $\mathrm{Re}_c = 1.3 \times 10^6$, $M = 0.14$, $\alpha = 6°$.

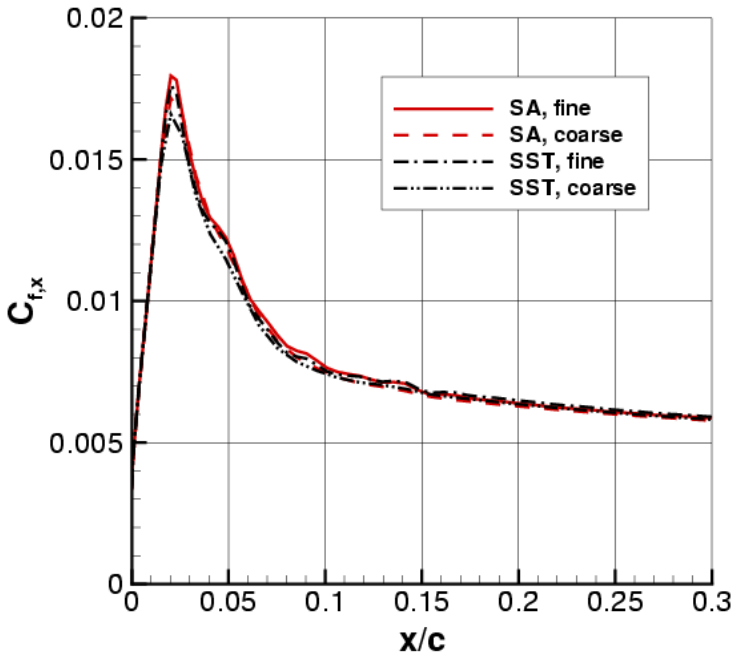

Figure 20. Computed x-direction component of skin friction coefficient on the upper surface of the main element of the NLR 7301 infinite swept wing, $\mathrm{Re}_c = 1.3 \times 10^6$, $M = 0.14$, $\alpha = 6°$.